AIChE

Numerical Simulation of Three-Dimensional Gas-Solid Particle Flow in a Horizontal Pipe

A. I. Kartushinsky
Research Laboratory of Multiphase Media Physics, Tallinn University of Technology, Tallinn 12618, Estonia

E. E. Michaelides
University of Texas at San Antonio, One UTSA Circle, San Antonio, TX 78249

Y. A. Rudi, S. V. Tisler, and I. N. Shcheglov
Research Laboratory of Multiphase Media Physics, Tallinn University of Technology, Tallinn 12618, Estonia

DOI 10.1002/aic.12528
Published online February 15, 2011 in Wiley Online Library (wileyonlinelibrary.com).

A three-dimensional model of particulate flows using the Reynolds Averaged Navier-Stokes method is presented. The governing equations of the gas–solids flow are supplemented with appropriate closure equations to take into account all the relevant forces exerted on the solid particles, such as particle-turbulence interactions, turbulence modulation, particle–particle interactions, particle–wall interactions, as well as gravitational, viscous drag, and lift forces. A finite volume numerical technique was implemented for the numerical solution of the problem. The method has been validated by comparing its results with the limited number of available experimental data for the velocity and turbulence intensity of the gas–particle flow. The results show that the presence of particles in the flow has a significant effect on all the flow variables. Most notably, the distribution of all the parameters becomes asymmetric, because of the gravitational effect on the particles and particle sedimentation. © 2011 American Institute of Chemical Engineers *AIChE J,* 57: 2977–2988, 2011
Keywords: diffusion (mass transfer, heat transfer), fluid mechanics, mathematical modeling, multiphase flow, numerical solutions

Introduction

Particulate confined flows and flows in channels have numerous engineering applications ranging from pneumatic conveying systems to coal gasifies and chemical reactors. They comprise one of the most thoroughly investigated subjects in the area of multiphase flow. Particulate flows are complex and are influenced by several physical variables, such as particle sedimentation, interparticle collisions, and particle forces, namely gravitational, lift, and drag forces.

For this reason, the early models of particulate flow were based on correlations or were simply phenomenological with the effects of several of these primary variables lumped together in several key flow parameters, such as the loading of the flow, or the density distribution of the multiphase mixture.[1,2] These models provide very useful practical/engineering information on the pressure drop or other quantities of practical interest, but do not provide any information on the details of the flow field, the distribution of the two phases or the effects of turbulence.[3]

A more thorough approach to the transport of solids in pipes was adopted in the 1980s when several of the primary flow parameters were investigated analytically or experimentally. Among these studies, the experimental results[4] showed that the decrease of the mean flow velocity in a horizontal channel results in the pronounced asymmetry of the distributions of all physical variables. These experiments also confirmed earlier empirical studies that a minimum mean flow velocity must be maintained for the particles to be transported

Correspondence concerning this article should be addressed to A. I. Kartushinsky at aleksander.kartusinski@ttu.ee.

or they will settle on the lower channel surface. The magnitude of this minimum transport velocity was examined by Davies[5] and Cabrejos and Klinzing.[6] The settling process and the asymmetry of the horizontal flow depend strongly on the transport velocity. High transport velocities imply no settling and almost symmetric flow distribution.

Almost symmetric distributions of the average and fluctuation velocities of the gas and the solid phase were observed in the horizontal pipe flow by Sommerfeld[7] at the rather high transport velocity of 18 m/s. Sommerfeld[7] also showed that the particle–wall and particle–particle collisions play an important role in the velocity field formation. He used a stochastic model of interparticle collisions[8] in which a fictitious particle with which the other particles collided was randomly introduced, using a random-number generator. A similar approach was used by Oesterle and Petitjean[9] and Tanaka and Tsuji[10] to illustrate the influence of interparticle collisions. However, the last study was restricted to a short pipe segment. Louge et al.[11] and Cao and Ahmadi[12] described the interparticle collisions within the Eulerian approach for particulate flow by means of the granular flow theory, which was originally promulgated by Gidaspov.[13]

A great deal of research has been also done on the subject of turbulence in particulate flows, where it was first ascertained that, in general, fine particles attenuated the turbulence intensity of the carrier fluid, whereas larger particles enhanced it.[14] Turbulence attenuation has been described quantitatively by a number of models, such as the ones by Yuan and Michaelides,[15] Yarin and Hetsroni,[16] and Crowe.[17] The latter study incorporated two turbulence modification mechanisms into a hybrid length and predicted fairly accurately the turbulence enhancement or attenuation in terms of the velocity slip and the loading. The Reynolds Averaged Navier-Stokes (RANS) model, presented here, uses the method[17] for simulating the turbulence modification phenomena.

There are a number of numerical studies published in recent years focusing on multiphase flows in confined flow domains. They are performed mostly within the frame of Eulerian-Lagrangian simulations. The simplified Euler–Euler model of Guet et al.[18] predicted the void fraction and velocity profiles in vertical upward bubbly pipe flows. The authors devised a method to compute the flow field with a large number of flow constraints associated with the effects of a gravitational pressure gradient. For a fully developed, axially symmetric flow, these conditions were reduced to a set of first-order equations that were solved with a fast convergence method. The Lagrangian particle tracking approach was performed for numerical simulation of bubbly flows by Göz et al.[19] These authors used a new numerical technique that allowed the tracking of heavy particles together with light solid particles in a fluid. Their analysis suggested the criteria for choosing an optimal time step to avoid numerical instabilities.

The 3-D and the time-dependent Euler-Lagrange simulations of the turbulent gas–solid flow in cyclone separators have been performed by Derksen et al.[20] The authors considered solid particles with different sizes, which are tracked by the LES method. The effect of particle-to-gas coupling on the gas-flow has taken into account even for low loadings, down to 0.2 loadings. The authors found that the presence of solid particles caused the damping of the swirl intensity in the cyclone with strongly attenuated turbulence. These two effects have had significant consequences for the performance of the cyclone. The collection efficiency responded in a more complicated manner to the mass loading, with mostly increased cut sizes, and increased overall efficiencies.

Among the more recent studies, Fairweather and Yao[21] studied the particle dispersion in a square duct flow. They applied the LES-Lagrange particle tracking method with one-way coupling and with a polydisperse particle composition. The authors showed that the small particles were much more influenced by the secondary flow and had almost uniformly distributed concentration. Also, deposition of large particles on the duct floor was observed. A detailed analysis of the flow influence on the particle's dispersion was performed in this study using a dynamical type of analysis.

One of the salient features of particulate flow is the radial dependence of axial velocities, which is caused by the action of gravity and is a more general manifestation of the "Boycott effect," which was observed during the process of sedimentation. Boycott[22] discovered this technique first by observing that oxalated or defibrinated blood corpuscles sediment much faster in an inclined tube than in a vertical one. During the sedimentation process with the Boycott effect, the particles first approach the inclined wall of the tube and form concentrated slurry, as leaving above them clear liquid. The slurry is significantly heavier than the clear liquid and slides along the inclined tube until it reaches the bottom.[23] Some features of the Boycott effect for gas–particle flows, which are associated with density waves in granular materials were examined experimentally by Raafat et al.,[24] who observed a nearly stationary structure of density waves, and numerically by Strauss et al.[25]

The description of two-phase gas–solid particle turbulent flows in horizontal channels is usually carried out by means of one- or two-dimensional models. For example, Kartushinsky and Michaelides[26] carried out the numerical simulation of the motion of particles within a frame of a two-phase turbulent boundary layer (TBL) approach by means of the decomposition of particulate flow onto the so-called falling and rebound particulate flows. This allowed them to derive numerically the asymmetric distributions of the longitudinal velocities of both phases and the turbulent energy profiles across the flow and also to derive other flow details and results that compared well with the experimental observations by Tsuji and Morikawa.[4] The flow asymmetry was apparent in the computations as well as the particle deposition and the saltation motion at the bottom wall of the channel.

It must be pointed out that the model by Kartushinsky and Michaelides[26] pertains to vertical, symmetric flows in pipes, whereas the one by Kartushinsky and Michaelides[27] uses the TBL approximation. Within that approximation and to examine the asymmetric distributions of the average velocity profiles of the gas and the dispersed phases, the particles were divided as "falling particles" and "rebounding particles." Thus, the previous approach introduced artificially different particles to take into account the interparticle collisions. The current model does not use the TBL approximation, calculates the radial and azimuthal velocities of the particles from conservation equations, and this does not make the use of the two types of "falling" and "rebound" particles. Thus, it is simpler, uses state of the art modeling and computational techniques, and it is more accurate because it does not use approximations. Thus, the present model uses a minimum number of assumptions and empiricism and

represents a more contemporary computational approach in turbulent particulate flow.

The theory of rapid granular flow has also been used recently to model and simulate gas–solid particle turbulent flow in vertical and inclined pipes. The study by Zhu et al.[28] was based on this theory and includes quantities such as the granular temperature, which may only be defined for the particulate phase. This work is simply based on the mechanical conservation equations, does not use the concept of granular temperature and uses the minimum set of mechanistic closure equations, which are necessary to solve the problem.

We used the two-fluid model for multiphase flows and applied it to relatively dilute flows. The addition of the concept of porosity and a porosity factor in the models would not be a problem when the flow is dense. However, for less than 10% volume concentrations, the addition of the porosity is not necessary. One of the advantages of this approach is that we have used closure equations (such as the turbulence modulation model) that may not be used in the framework of the rapid granular flow model. Another advantage is that one may account for both the effects of particle-turbulence interaction and the interparticle collisions, within the same model and with closure equations that are compatible. With this, we can observe the turbulent diffusion of the particles at the same time as the particle dispersion, which is due to particulate interactions. The fluid viscosity moderates both of these processes as well as the turbulence of the entire flow.

As there are only a few studies related to the three-dimensional modeling of particulate flows that are based on the Eulerian description of the dispersed phase, the present model and the accompanying analysis and computations will be of interest to scientists and engineers that model granular and particulate flows in horizontal channels.

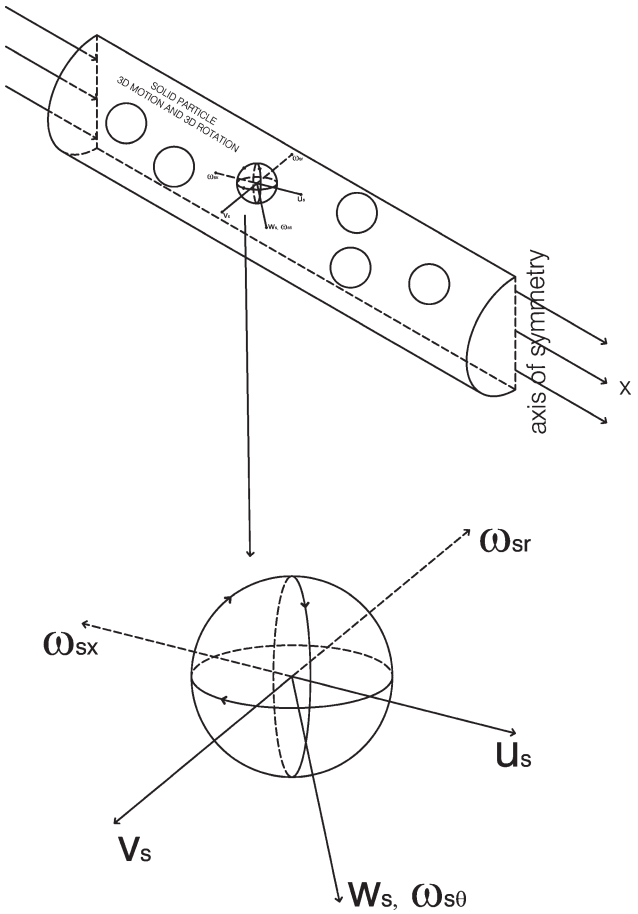

Figure 1. Schematic diagram of the flow configuration and velocities of solid particles.

Governing Equations

Figure 1 depicts a schematic diagram of the three-dimensional pipe flow and shows explicitly the linear and angular velocities of the solid phase within the two phase mixture in the pipe.

Continuity equation of the fluid phase

$$\frac{\partial}{\partial x}(ru)+\frac{\partial}{\partial r}(rv)+\frac{\partial w}{\partial \theta}=0 \tag{1}$$

where u, v, and w are the longitudinal, radial, and azimuthal velocity components of the gas phase, respectively.

Longitudinal linear momentum equation of the fluid phase

$$\begin{aligned}&\frac{\partial}{\partial x}r\left[u^2-\tilde{\nu}_t\frac{\partial u}{\partial x}\right]+\frac{\partial}{\partial r}r\left[uv-\tilde{\nu}_t\frac{\partial u}{\partial r}\right]+\frac{\partial}{\partial \theta}\left[uw-\tilde{\nu}_t\frac{\partial u}{r\partial \theta}\right]\\&=\frac{\partial}{\partial x}\left(\tilde{\nu}_t r\frac{\partial u}{\partial x}\right)+\frac{\partial}{\partial r}\left(\tilde{\nu}_t r\frac{\partial v}{\partial x}\right)+\frac{\partial}{\partial \theta}\left(\tilde{\nu}_t\frac{\partial w}{\partial x}\right)\\&-\frac{r\partial p}{\rho\partial x}-\alpha r\left[\frac{u_r}{\tau'_p}+v_r(C_M\Omega_\theta+f_s\omega_\theta)-w_r(C_M\Omega_r+f_s\omega_r)\right],\end{aligned} \tag{2}$$

where $\tilde{\nu}_t=\nu_t+\nu$ is the turbulent viscosity, which is the sum of the turbulent and laminar viscosities; the turbulent viscosity is calculated from the expression $\nu_t=c_\mu\sqrt{k}L_0$ with $c_\mu=0.09$ (c_μ is numerical constant from $k-\varepsilon$ model); k is the turbulent kinetic energy, and L_0 is the integral length scale of single-phase flow defined by Crowe[17]; p is the pressure; α is the mass concentration; $u_r=u-u_s$, $v_r=v-v_s$, and $w_r=w-w_s$ are the velocity differences between the gas and the dispersed phase occurring in the axial, radial, and azimuthal directions, respectively; $\tau'_p=\frac{\tau_p}{C'_D}$ is a particle response time that specifies the drag for the motion of the particles in the non-Stokesian regime: $C'_D=1+0.15Re_s^{0.687}$ with the particle Reynolds number given by the expression: $Re_s=\frac{\delta\sqrt{u_r^2+v_r^2+w_r^2}}{\nu}=\frac{\delta|\vec{V}_r|}{\nu}$.[29] The Stokesian[3] particle response time, τ_p, is $\tau_p=\left(\frac{18\rho\nu}{\rho_p\delta^2}\right)^{-1}$; ρ and ρ_p are the densities of air and particle, respectively, and δ is the particle size. If the solids mixture is polydisperse, then a momentum equation is solved for each fraction, whose diameter is denoted by δ_i or the equivalent diameter for irregular particles[30] and the material density by ρ_{pi}.[3]

The Magnus lift force is calculated from the expression: $\vec{F}_M=\frac{\rho}{2}|\vec{V}_r|C_L\frac{\pi\delta^2\vec{V}_r\times\vec{\Omega}}{4|\vec{\Omega}|}$, with the angular slip velocity calculated in the cylindrical coordinates from the expression:

$$\vec{\Omega} = \Omega_x\vec{i} + \Omega_r\vec{j} + \Omega_\theta\vec{k} = \vec{\omega}_s - 0.5\mathrm{rot}\vec{V} = \vec{\omega}_s - 0.5\left\{\frac{1}{r}\left[\frac{\partial(rw)}{\partial r} - \frac{\partial v}{\partial\theta}\right]\vec{i} + \left[\frac{1}{r}\frac{\partial w}{\partial\theta} - \frac{\partial w}{\partial x}\right]\vec{j} + \left[\frac{\partial v}{\partial x} - \frac{\partial u}{\partial r}\right]\vec{k}\right\}$$

where the ort-vectors $\vec{i}$, $\vec{j}$, and $\vec{k}$ are in the streamwise, radial, and azimuthal directions, respectively, and $\vec{\omega}_s = \omega_{sx}\vec{i} + \omega_{sr}\vec{j} + \omega_{s\theta}\vec{k}$ is the angular velocity of a solid fraction. For the closure equations, the coefficient of Magnus lift force is calculated by the closure equation: $C_M = \frac{\rho C_L|\vec{V}_r|}{\rho_p\delta|\vec{\Omega}|}$, with the lift coefficient given as $C_L = \min(0.5, 0.5\chi)$, where the parameter χ_i is defined as: $\chi = \frac{\delta|\vec{\omega}_s|}{|\vec{V}_r|}$.[3,31] f_s is the coefficient for the so-called Saffman force, which is due to the local shear of the flow. This coefficient is given by the closure equation: $f_s = \frac{3.07\cdot\rho\psi}{\rho_p\delta}\sqrt{\frac{\nu}{|\mathrm{rot}\vec{V}|}}\left(\vec{V}_r \times \mathrm{rot}\vec{V}\right)$, and the correction ψ has been calculated by Mei[32] as follows:

$$\psi = \begin{cases} 1 - 0.3314\sqrt{\beta}\exp(-0.1Re_s) + 0.3314\sqrt{\beta} & Re_s \le 40 \\ 0.0524\sqrt{\beta Re_s} & Re_s > 40 \end{cases}$$

with $\beta = \frac{\delta|\mathrm{rot}\vec{V}|}{2|\vec{V}_r|}$ in the range: $0.005 < \beta < 0.4$.

The lift force is a consequence of Newton's second law. It appears in particulate flows whenever there is shear and must be included in the balance of forces for the particles. In our modeling, the particles move mainly under impact of four force factors: the viscous drag, gravitation, lift forces, and turbulent diffusion. Another variable that may provide "lift" near a boundary is the slip velocity at the wall, which was used by Zhu et al.[28] It appears that in the model[28] this effect as well as the turbulent diffusion of particles near the wall compensated for the missing lift force.

Radial linear momentum equation of the fluid phase

$$\frac{\partial}{\partial x}r\left[uv - \tilde{\nu}_t\frac{\partial v}{\partial x}\right] + \frac{\partial}{\partial r}r\left[v^2 - \tilde{\nu}_t\frac{\partial v}{\partial r}\right] + \frac{\partial}{\partial\theta}\left[vw - \tilde{\nu}_t\frac{\partial v}{r\partial\theta}\right] = \frac{\partial}{\partial x}\left(\tilde{\nu}_t r\frac{\partial u}{\partial r}\right) + \frac{\partial}{\partial r}\left(\tilde{\nu}_t r\frac{\partial v}{\partial r}\right) + \frac{\partial}{\partial\theta}\left(\tilde{\nu}_t\frac{\partial w}{\partial r}\right) - 3\tilde{\nu}_t\frac{\partial w}{r\partial\theta} + \left(w - \frac{\partial\tilde{\nu}_t}{r\partial\theta}\right) - \frac{2\tilde{\nu}_t v}{r} - \frac{r\partial p}{\rho\partial r} - \alpha r\left[\frac{v_r}{\tau'_p} + w_r(C_M\Omega_x + f_s\omega_x) - u_r(C_M\Omega_\theta + f_s\omega_\theta)\right], \quad (3)$$

It must be pointed out that since the full Navier-Stokes equations are used in this model the radial momentum equation is not simply reduced to a vanishing average transverse velocity.[27] This full modeling of the radial velocity, rather than take a shortcoming, is one of the advantages of using the RANS method. It must notice, however, that the magnitude of the radial velocity is expected to be significantly smaller than that of the axial velocity.

Azimuthal linear momentum equation of fluid phase

$$\frac{\partial}{\partial x}r\left[uw - \tilde{\nu}_t\frac{\partial w}{\partial x}\right] + \frac{\partial}{\partial r}r\left[vw - \tilde{\nu}_t\frac{\partial w}{\partial r}\right] + \frac{\partial}{\partial\theta}\left[w^2 - \tilde{\nu}_t\frac{\partial w}{r\partial\theta}\right] = \frac{\partial}{\partial x}\left[\tilde{\nu}_t\frac{\partial u}{\partial\theta}\right] + \frac{\partial}{\partial r}\left[\tilde{\nu}_t\frac{\partial v}{\partial\theta}\right] + \frac{\partial}{\partial\theta}\left[\tilde{\nu}_t\frac{\partial w}{r\partial\theta}\right] - \left[v + \frac{\tilde{\nu}_t}{r} + \frac{\partial\tilde{\nu}_t}{\partial r}\right]w + \frac{3\tilde{\nu}_t\partial v}{r\partial\theta} + 2\nu\frac{\partial\tilde{\nu}_t}{r\partial\theta} - \frac{\partial p}{\rho\partial\theta} - \alpha r\left[\frac{w_r}{\tau'_p} + u_r(C_M\Omega_r + f_s\omega_r) - v_r(C_M\Omega_x + f_s\omega_x)\right]. \quad (4)$$

As with the momentum equation in the radial direction, the effects of the fluid phase rotation, the Magnus force, and the Saffman force effected on the particles are explicitly taken into account.

Turbulent kinetic energy equation of the fluid phase

$$\frac{\partial(rvk)}{r\partial r} + \frac{\partial(wk)}{r\partial\theta} + \frac{\partial(uk)}{\partial x} = \frac{\partial}{r\partial r}\left(\frac{\nu_t}{\sigma_k}r\frac{\partial k}{\partial r}\right) + \frac{\partial}{r\partial\theta}\left(\frac{\nu_t}{\sigma_k}\frac{\partial k}{r\partial\theta}\right) + \frac{\partial}{\partial x}\left(\frac{\nu_t}{\sigma_k}\frac{\partial k}{\partial x}\right) + P_k - \varepsilon_h + \frac{\alpha}{\tau_p}\left[u_r^2 + v_r^2 + w_r^2 + 0.5k_s - \frac{2k\tau_p}{(\tau_p + T_0)}\right], \quad (5)$$

where the production term describes the generation of the turbulent energy caused by the velocity gradient of gas, P_k. This term is given by the following closure equation:

$$P_k = \nu_t\left\{2\left[\left(\frac{\partial v}{\partial r}\right)^2 + \left(\frac{\partial u}{\partial x}\right)^2 + \left(\frac{\partial w}{r\partial\theta} + \frac{v}{r}\right)^2\right] + \left[\left(\frac{\partial w}{\partial r} - \frac{w}{r} + \frac{\partial v}{r\partial\theta}\right)^2 + \left(\frac{\partial v}{\partial x} + \frac{\partial u}{\partial r}\right)^2 + \left(\frac{\partial u}{r\partial\theta} + \frac{\partial w}{\partial x}\right)^2\right]\right\}, l$$

where $k = 0.5\left(\overline{u'^2} + \overline{v'^2} + \overline{w'^2}\right)$ is the turbulent kinetic energy; $\varepsilon_h = \frac{k\sqrt{k}}{L_h}$ is the rate of dissipation, which is computed according to the four-way coupling model[17] using the definition of a hybrid length scale $L_h = \frac{2L_0\lambda}{L_0+\lambda}$. L_h is the harmonic average of the integral length scale of single-phase flow L_0 and an average interparticle distance, $\lambda = \left(\sqrt[3]{\frac{\pi\rho_p}{6\rho\alpha}} - 1\right)\delta$. $k_s = 0.5\left(\overline{u_s'^2} + \overline{v_s'^2} + \overline{w_s'^2}\right)_c$ is the collision energy of particles and is computed according to the model.[33] The last term in the right-hand side of Eq. 5 takes into account the turbulent kinetic energy attenuation by the particles. It is computed according to Pourahmadi and Humphrey[34] with the turbulent integral time scales of single phase being given as $T_0 = 0.3\frac{k_0}{\varepsilon_0}$, σ_k is a numerical constant in the $k - \varepsilon$ model, equal to $\sigma_k = 1$.

The most commonly used turbulence modulation model for particulate flows is the one by Crowe,[17] which takes into account the influence of particles on the gas turbulence. The main difference of the model[17] from the so-called "classical" $k - \varepsilon$ is that it includes only one differential equation, the one for the turbulent specific kinetic energy, k. The

dissipation rate for this model is calculated by the turbulence macroscale, which depends on the dissipation rate of the single phase flow and the interparticle distance, λ. The main contribution of the particle feedback to the turbulence of the carrier fluid is determined by the following:

1. the square of velocity lag between the average velocities of the carrier fluid and the dispersed phase and

2. by the interparticle distance, λ, which is a measure of the concentration of particles.

This additional turbulence enhancement is balanced by the dissipation of the turbulent energy determined by the harmonic length, L_h. This k–L model gives accurate results in the two-phase turbulent pipe flows.[26,33] It must be noted that k–L model stems from the $k-\varepsilon$ model and it is essentially the adaptation of the latter to particulate flows by the introduction of the harmonic turbulence scale L_h which is calculated by interparticle distance λ. Thus, the k–L model captures the particle feedback on the turbulence, which the classical $k-\varepsilon$ does not without an ad hoc tuning/calibration of the model constants. For example, the classical k–ε model when used with particulate flows[35] suffers from the problem of the description of the turbulence generation term. The latter is simply proportional to the square of the velocity slip between phases in k–L model. In this article, we performed some calculations with the classical $k-\varepsilon$ model and compared them with the results of the k–L model.

For this reason, we prefer to use the k–L model rather than $k-\varepsilon$ model for the modeling of the particulate turbulent flows.

Continuity equation of the dispersed phase

$$\frac{\partial}{\partial x}\alpha\tilde{u}_s+\frac{\partial}{r\partial r}r\alpha\tilde{v}_s+\frac{\partial}{r\partial\theta}\alpha\tilde{w}_s=0 \tag{6a}$$

where $\tilde{u}_s$, $\tilde{v}_s$, and $\tilde{w}_s$ are the longitudinal, radial, and azimuthal components of the particles drift velocity, respectively, and are given by the following equations:

$$\tilde{u}_s=u_s-\left(D_t+D_c^x\right)\frac{\partial\ln\alpha}{\partial x},\ \tilde{v}_s=v_s-\left(D_t+D_c^r\right)\frac{\partial\ln\alpha}{\partial r},\quad \tilde{w}_s=w_s-\left(D_t+D_c^\theta\right)\frac{\partial\ln\alpha}{r\partial\theta}. \tag{6b}$$

The given expressions for the longitudinal, radial, and azimuthal components of the particle velocities consist of the two parts: the linear velocity itself and the drift velocity. The latter is the result of the diffusion of particles and is due to the nonuniform distribution of the particle concentration along the flow domain.

The coefficient of the particle turbulent diffusion D_t that takes into accounts the influence of the turbulent motion of the gas on the dispersion of the particles is calculated according to the model[35]:

$$D_t=\frac{2k}{3}L_0\frac{\left[\sqrt{\frac{2}{3}k}+0.5\left(\left|\vec{V}_r\right|+\frac{u_\tau^2}{\left|\vec{V}_r\right|}\right)\right]}{\left(\sqrt{\frac{2}{3}k}+\left|\vec{V}_r\right|\right)^2} \tag{6c}$$

The pseudoviscosity diffusion coefficients in the longitudinal, D_c^x, radial, D_c^r, and azimuthal, D_c^θ directions are results of the particle collisions, and they are not constants and calculated analytically according to the model by Kartushinsky and Michaelides.[33]

Longitudinal linear momentum equation of the dispersed phase

$$\begin{aligned}\frac{\partial}{\partial x}\alpha r\left[u_s\tilde{u}_s-\tilde{\nu}_s\frac{\partial u_s}{\partial x}\right]+\frac{\partial}{\partial r}\alpha r\left[u_s\tilde{v}_s-\tilde{\nu}_s\frac{\partial u_s}{\partial r}\right]+\frac{\partial}{\partial\theta}\alpha\left[u_s\tilde{w}_s-\tilde{\nu}_s\frac{\partial u_s}{r\partial\theta}\right]=\frac{\partial}{\partial x}\left(\tilde{\nu}_s r\frac{\partial u_s}{\partial x}\right)\\+\frac{\partial}{\partial r}\left(\tilde{\nu}_s r\frac{\partial v_s}{\partial x}\right)+\frac{\partial}{\partial\theta}\left(\tilde{\nu}_s\frac{\partial w_s}{\partial x}\right)+\alpha r\left[\frac{u_r}{\tau_p'}+v_r(C_M\Omega_\theta+f_s\omega_\theta)-w_r(C_M\Omega_r+f_s\omega_r)\right],\end{aligned} \tag{7}$$

where $\tilde{\nu}_s=\nu_{st}+\nu_{sc}$ is the pseudoviscosity coefficient of the dispersed phase calculated as coefficient due to the particles involvement into turbulent motion by model of Zaichik and Alipchenkov[36] as $\nu_{st}=\left(\nu+\frac{\tau k}{3}\right)\left[1-\exp\left(-\frac{T_0}{\tau_\eta}\right)\right]$ and calculated due to interparticle collisions by the model.[33]

Radial linear momentum equation of the dispersed phase

$$\begin{aligned}\frac{\partial}{\partial x}r\alpha\left[v_s\tilde{u}_s-\tilde{\nu}_s\frac{\partial v_s}{\partial x}\right]+\frac{\partial}{\partial r}r\alpha\left[v_s\tilde{v}_s-\tilde{\nu}_s\frac{\partial v_s}{\partial r}\right]+\frac{\partial}{\partial\theta}\left[v_s\tilde{w}_s-\tilde{\nu}_s\frac{\partial v_s}{r\partial\theta}\right]=\frac{\partial}{\partial x}\left(\tilde{\nu}_s r\frac{\partial u_s}{\partial r}\right)+\frac{\partial}{\partial r}\left(\tilde{\nu}_s r\frac{\partial v_s}{\partial r}\right)\\+\frac{\partial}{\partial\theta}\left(\tilde{\nu}_s\frac{\partial w_s}{\partial r}\right)-3\tilde{\nu}_s\frac{\partial w_s}{r\partial\theta}+\left(w_s-\frac{\partial\tilde{\nu}_s}{r\partial\theta}\right)-\frac{2\tilde{\nu}_s v_s}{r}+r\alpha\left[\frac{v_r}{\tau_p'}+g\left(1-\frac{\rho}{2\rho_p}\right)\cos\theta+w(C_M\Omega_x+f_s\omega_x)\right.\\\left.-u_r(C_M\Omega_\theta+f_s\omega_\theta)\right],\end{aligned} \tag{8}$$

where g is the acceleration of gravity.

Azimuthal linear momentum equation of the dispersed phase

$$\begin{aligned}\frac{\partial}{\partial x}r\alpha\left[w_s\tilde{u}_s-\tilde{\nu}_s\frac{\partial w_s}{\partial x}\right]+\frac{\partial}{\partial r}r\alpha\left[w_s\tilde{v}_s-\tilde{\nu}_s\frac{\partial w_s}{\partial r}\right]+\frac{\partial}{\partial\theta}\alpha\left[w_s\tilde{w}_s-\tilde{\nu}_s\frac{\partial w_s}{r\partial\theta}\right]=\frac{\partial}{\partial x}\left[\tilde{\nu}_s\frac{\partial u_s}{\partial\theta}\right]\\+\frac{\partial}{\partial r}\left[\tilde{\nu}_s\frac{\partial v_s}{\partial\theta}\right]+\frac{\partial}{\partial\theta}\left[\tilde{\nu}_s\frac{\partial w_s}{r\partial\theta}\right]-\left[v_s+\frac{\tilde{\nu}_s}{r}+\frac{\partial\tilde{\nu}_s}{\partial r}\right]w_s+\frac{3\tilde{\nu}_s\partial v_s}{r\partial\theta}+2v_s\frac{\partial\tilde{\nu}_s}{r\partial\theta}-r\alpha\left[\frac{w_r}{\tau_p'}+g\left(1-\frac{\rho}{2\rho_p}\right)\sin\theta\right.\\\left.+u_r(C_M\Omega_r+f_s\omega_r)-v_r(C_M\Omega_x+f_s\omega_x)\right].\end{aligned} \tag{9}$$

Angular momentum equation of the dispersed phase in the longitudinal direction

$$\frac{\partial}{\partial x}\alpha r\left[\omega_{sx}\tilde{u}_s-\tilde{\nu}_s^{\omega}\frac{\partial\omega_{sx}}{\partial x}\right]+\frac{\partial}{\partial r}\alpha r\left[\omega_{sx}\tilde{v}_s-\tilde{\nu}_s^{\omega}\frac{\partial\omega_{sx}}{\partial r}\right]+\frac{\partial}{\partial\theta}\alpha\left[\omega_{sx}\tilde{w}_s-\tilde{\nu}_s^{\omega}\frac{\partial\omega_{sx}}{r\partial\theta}\right]=-\alpha C_{\omega}\frac{\Omega_x}{\tau_p} \quad (10)$$

where $\tilde{\nu}_s^{\omega}=\nu_{st}+\nu_{sc}^{\omega}$, ν_{st} is the turbulent viscosity coefficient of particles involved into the turbulent motion, and ν_{sc}^{ω} is the coefficient of the collisional pseudoviscosity calculated according to the model.[33] The additional terms in the equations of the dispersed phase are the pseudodiffusion coefficients, D_c^x, D_c^r, D_c^{θ}, which are in Eq. 6b, and the pseudoviscosity coefficients, ν_{sc}, ν_{sc}^{ω}, in Eqs. 7–10. These terms are obtained analytically from Kartushinsky and Michaelides[33] and take into account the interparticle collisions. These collisions are important, especially at the bottom of the pipe, where particle accumulation is always observed. In the calculations, we applied the particle distribution function model of Zaichik and Alipchenkov[36] to derive the coefficients ν_{st}.

The right-hand side of Eq. 10 takes into account the torque in the longitudinal direction due to the viscosity of fluid phase. According to Happel and Brenner,[37] the coefficient $C_{\omega}=\frac{10}{3}$.

Angular momentum equation of the dispersed phase in the radial direction

$$\frac{\partial}{\partial x}\alpha r\left[\omega_{sr}\tilde{u}_s-\tilde{\nu}_s^{\omega}\frac{\partial\omega_{sr}}{\partial x}\right]+\frac{\partial}{\partial r}\alpha r\left[\omega_{sr}\tilde{v}_s-\tilde{\nu}_s^{\omega}\frac{\partial\omega_{sr}}{\partial r}\right]+\frac{\partial}{\partial\theta}\alpha\left[\omega_{sr}\tilde{w}_s-\tilde{\nu}_s^{\omega}\frac{\partial\omega_{sr}}{r\partial\theta}\right]=-\alpha C_{\omega}\frac{\Omega_r}{\tau_p} \quad (11)$$

Angular transfer equation of the dispersed phase in the azimuthal direction

$$\frac{\partial}{\partial x}\alpha r\left[\omega_{s\theta}\tilde{u}_s-\tilde{\nu}_s^{\omega}\frac{\partial\omega_{s\theta}}{\partial x}\right]+\frac{\partial}{\partial r}\alpha r\left[\omega_{s\theta}\tilde{v}_s-\tilde{\nu}_s^{\omega}\frac{\partial\omega_{s\theta}}{\partial r}\right]+\frac{\partial}{\partial\theta}\alpha\left[\omega_{s\theta}\tilde{w}_s-\tilde{\nu}_s^{\omega}\frac{\partial\omega_{s\theta}}{r\partial\theta}\right]=-\alpha C_{\omega}\frac{\Omega_{\theta}}{\tau_p} \quad (12)$$

Equations 10–12 result from the three-dimensionality of the particles rotation, which is caused by the fluid viscosity, collisions, and other effects.

One of the novelties of this model is the transition from the two-dimensional to the three-dimensional particulate flow model. The well-known equations of the three-dimensional single-phase flows are extended to the three-dimensional particulate flows using the following common assumptions:

1. there is no hydrostatic pressure for the dispersed phase,

2. the expressions written for the viscosity terms of the single-phase and the dispersed phases are different because they take into account the particle influence on the fluctuating turbulent motion, and

3. there is a velocity slip along the walls for the particulate flow, which results from the particles inertia and the collision processes with the wall.

All the velocities of carrier fluid and solid phase are according to the practice of the RANS modeling that is we used Favre's time average equations for the gas phase and the dispersed phase. The two phases are coexisting phases in the flow domain (two-fluid model). For the solution, we considered initially stationary conditions but not steady-state conditions. The flow was developed during calculations up to 50 pipe diameters and became fully developed flow.

Boundary Conditions

It is assumed that the particles enter the pipe into a developed and previously computed single-phase velocity field. The particles are introduced with a lesser velocity, which is characterized by a lag coefficient, k_{lag}, being uniform in all directions:

$$x=0,\quad u_s=k_{lag}u,\quad v_s=k_{lag}v,\quad w_s=k_{lag}w,\quad \omega_{sx}=\omega_{sr}=0,\quad \omega_{s\theta}=k_{lag}(0.5\nabla\times\vec{v}) \quad (13)$$

Because the particles deposit onto the bottom wall of the pipe, the symmetrical boundary conditions at the pipe axis do not apply for $r=0$. Therefore, we bring into consideration the elementary volume of the flow field, which is located near the point $r=0$ and calculated by the grid mesh. The flow parameters are calculated for the given volume element at $r=0$ by integration over the azimuthal coordinate, $\langle f(x,\Delta r)\rangle|_{\theta}=\int_0^{\pi}f(x,\Delta r,\theta)d\theta$. Thus, the obtained linear and angular velocities of both phases, the particle mass concentration, and the turbulent kinetic energy have the values which are not equal to their adjacent values located at one mesh size grid off $r=0$.

Thus, the asymmetrical pipe flow conditions at $r=0$ look like:

$$\begin{aligned}
&r=0: u=\langle u(x,\Delta r)\rangle|_{\theta},\quad v=\langle v(x,\Delta r)\rangle|_{\theta},\\
&w=\langle w(x,\Delta r)\rangle|_{\theta},\\
&u_s=\langle u_s(x,\Delta r)\rangle|_{\theta},\quad v_s=\langle v_s(x,\Delta r)\rangle|_{\theta}\\
&w_s=\langle w_s(x,\Delta r)\rangle|_{\theta},\quad \alpha=\langle\alpha(x,\Delta r)\rangle|_{\theta},\\
&\omega_{sx}=\langle\omega_{sx}(x,\Delta r)\rangle|_{\theta},\quad \omega_{sr}=\langle\omega_{sr}(x,\Delta r)\rangle|_{\theta},\\
&\omega_{s\theta}=\langle\omega_{s\theta}(x,\Delta r)\rangle|_{\theta},\\
&k=\langle k(x,\Delta r)\rangle|_{\theta}.
\end{aligned} \quad (14)$$

At the wall vicinity the nonslip condition is applied by the wall function approach in a way that is similar to the methods.[38,39] These methods were adapted to the control volume applications:

$$\begin{aligned}
&r=R: u^+=\frac{u}{u_{\tau}}=\frac{1}{\kappa}\ln y^+ +5.2, v=w=0,\\
&u_{\tau}=\sqrt{\frac{\kappa\cdot c_{\mu}^{0.25}u\cdot\left(\frac{\overline{u'^2}+\overline{v'^2}+\overline{w'^2}}{2}\right)^{0.5}}{\ln(E\cdot y^+)}}=\sqrt{\frac{\kappa\cdot c_{\mu}^{0.25}u\cdot k^{0.5}}{\ln(E\cdot y^+)}},\\
&\kappa=0.41, E=8.43171.
\end{aligned} \quad (15)$$

The slip boundary condition is prescribed for the dispersed phase along the wall as the first step in the calculations, according to Ding et al.[40] For the subsequent computations, the parameters of the particle–wall interactions are determined according to the model.[41] Regarding these interactions, one of the two cases is possible:

a. sliding collision and

b. nonsliding collision.

These two cases are characterized by the appropriate values of the restitution coefficient, k_n, and the friction coefficient, f.

The boundary conditions set at the wall in case of the sliding collision are as follows:

$$r = R : u_s = -\lambda \frac{\partial u_s}{\partial r}, v_s = -\lambda \frac{\partial v_s}{\partial r},$$
$$w_s = -\lambda \frac{\partial w_s}{\partial r}, \frac{\partial \alpha}{\partial r} = 0, \omega_{sx} = \lambda \frac{\partial \omega_{sx}}{\partial r}, \omega_{sr} = 0 \qquad (16)$$
$$\omega_{s\theta} = \lambda \frac{\partial \omega_{s\theta}}{\partial r},$$

where the interparticle spacing is given by the closure equation according to Crowe et al.[31] as: $\lambda = \delta\left\{\left[\frac{\pi}{6}\left(\frac{\rho_p}{\rho\alpha}+1\right)\right]^{1/3}-1\right\}$.

The last expression allows the imposition of the boundary condition for the dispersed phase as the "sliding" condition of particles along the wall.[40] Thus, when the particles come in contact with the wall they do not stop, but are allowed to have a finite velocity component in the longitudinal direction along the wall. The sliding is due to a combination of the particles' inertia and gravity forces that apply near the pipe walls. Thus, when the particles collide with the bottom wall, their linear and angular velocities are recalculated according to Kartushinsky and Michaelides.[26] The same boundary conditions are set for both phases at the top ($\theta = 0$) and the bottom ($\theta = \pi$) halves of the flow domain:

$$\theta = 0 : \frac{\partial u}{\partial \theta} = \frac{\partial k}{\partial \theta} = \frac{\partial u_s}{\partial \theta} = \frac{\partial \alpha}{\partial \theta} = \frac{\partial \omega_{sr}}{\partial \theta}$$
$$= v = w = v_s = w_s = \omega_{sx} = \omega_{s\theta} = 0, \qquad (17a)$$

$$\theta = \pi : \frac{\partial u}{\partial \theta} = \frac{\partial k}{\partial \theta} = \frac{\partial u_s}{\partial \theta} = \frac{\partial \alpha}{\partial \theta} = \frac{\partial \omega_{sr}}{\partial \theta}$$
$$= v = w = v_s = w_s = \omega_{sx} = \omega_{s\theta} = 0, \qquad (17b)$$

The exit of the cylindrical channel, where the flow reaches a steady state, is assumed to be at $x = 50D$. The following boundary conditions define the steady state:

$$x = 50D : \frac{\partial u}{\partial x} = \frac{\partial v}{\partial x} = \frac{\partial u_s}{\partial x} = \frac{\partial v_s}{\partial x} = \frac{\partial w_s}{\partial x} = \frac{\partial \omega_{sx}}{\partial x} = \frac{\partial \omega_{sr}}{\partial r}$$
$$= \frac{\partial \omega_{s\theta}}{\partial r} = \frac{\partial \alpha}{\partial x} = \frac{\partial k}{\partial x} = 0. \qquad (18)$$

Numerical Method

The control volume method is applied to solve the governing differential equations numerically. The governing equations were solved using the ILU method, which incorporates a strong, implicit procedure with lower and upper matrix decomposition,[39] and with flux- blended and deferred correction scheme, which was first used by Perić and Scheuerer.[38] Approximately 31,360,000 control volumes were used with equal grid sizes along the axial, radial, and azimuthal directions. The number of control volumes along the radial direction is 28, the number of control volumes along the azimuthal direction is 40, and the number along the axial direction is 2,800. The later coincides with a distance of 50 radii along the horizontal pipe. To use the wall functions as the boundary conditions, one step from the wall boundaries has been chosen as the starting point of the wall functions with the logarithmic velocity distribution for the gas phase. The friction velocity v_* was calculated through the turbulent kinetic energy equation, as a result of the balance of the kinetic energy production and its dissipation in the vicinity of the wall at the distance $y^+ = 11.6$, as recommended by Perić and Scheuerer.[38]

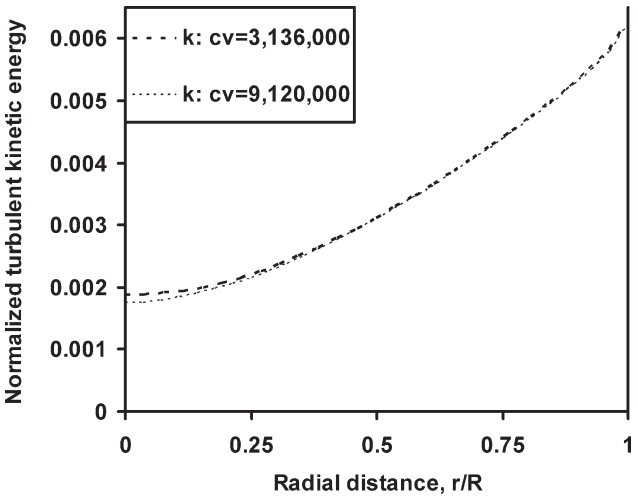

Figure 2. Normalized turbulent energy profiles of the gas phase for two numbers of finite volumes (fv): 3,136,000 and 9,120,000.

The mean transport velocity is 6 m/s.

Because the flow is asymmetric, the entire solution process is computationally intensive and each computation requires up to 1 week of CPU time in a Sun processor. We performed a grid independence test and made computations for two different numbers of finite volumes with (a) 3,136,000 and (b) 9,120,000.

The numerical results are presented in Figures 1 and 2 for the k-profiles (turbulent energy) and for the particle mass concentration. It is evident that the behavior of these basic flow parameters is almost insensitive to this change of the numbers of finite volumes, which implies that the use of 3,136,000 volumes is sufficient for the convergence of the numerical method and derivation of accurate results. For this reason, we adopted the value of 3,136,000 control volumes for the computations that follow.

Results and Discussion

All the numerical results that appear in the following plots have been obtained at the exit of the pipe, which is at $x/D = 50$ with $D = 0.0305$ m. The results are presented in dimensionless form with all the velocities and kinetic energies

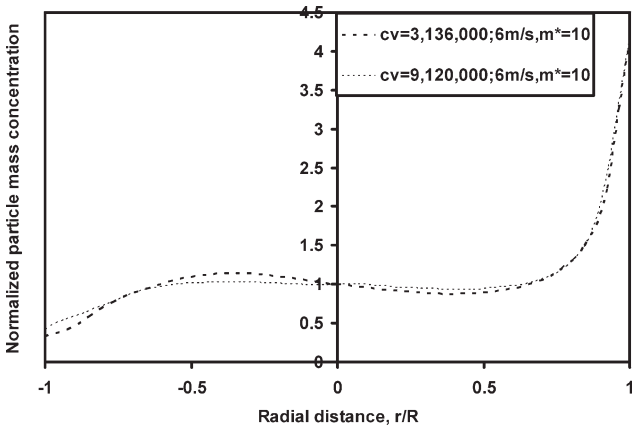

Figure 3. Normalized particle mass concentration profiles of the gas phase for two grids with numbers of finite volumes (fv): 3,136,000 and 9,120,000.

The mean transport velocity is 6 m/s and $m^* = 10$.

reduced by the gaseous velocity at the centerline u_m. The area-averaged gas velocity $\bar{u}$ varies from 6 to 15 m/s and this yields a change for the Reynolds number from 12,000 to 30,000. Unless otherwise specified, the calculations used relatively light, monodisperse spherical polystyrene particles with material density $\rho_p = 1{,}020$ kg/m^3 and mean particle size of $5 = 0.21$ mm. Two mass loadings were considered, $m^* = 2.5$ and $m^* = 10$. Collisions in such monodisperse particulate mixtures occur mainly because of the fluctuating particle velocities. Additional collisions occur at the bottom of the cylindrical channel, where particles accumulate and their concentration is significantly higher than the average.

In all given figures, there are plots across the whole cross section of flow from top ($y = -1$) to the bottom ($y = +1$) through the pipe center, whereas the azimuthal angle that changes from 0 at top wall surface to 180° at bottom wall surface passing by mid cross section at angle 90°.

The Figure 3 shows normalized particle mass concentration profiles for two numbers of finite volumes (fv): 3,136,000 and 9,120,000 for the mean transport velocity of 6 m/s and mass loading $m^* = 10$. A glance at Figures 2 and 3 shows that the results with the finer grid are almost identical to the ones of the coarser grid. From the two figures, one may conclude that the grid with 3,136,000 finite volumes is sufficient for the convergence of the numerical scheme and yields accurate results.

Figures 4 and 5 depict the longitudinal profiles of the gaseous phase velocity and the particle phase velocity using two average gas transport velocities, $\bar{u} = 15$ and 6 m/s and two mass loading of the flow: $m^* = 2.5$ and 10. The top of the channel is at $r/R = -1$ and the bottom at $r/R = 1$. It is apparent that the effect of gravity on the particles causes an asymmetric velocity profile for both phases, with a maximum slightly above the centerline. The experimental data[4] are also shown in the figure. It is observed that the experimental data agree well with the numerical computations for the same loading, because the difference between the computational results and the experimental data is well within the experimental uncertainty of the data. It is also observed that the asymmetry of the flow is more pronounced in the case of the lower velocity (6 m/s), where it is expected that a higher number of particles fall to the bottom of the pipe and move by saltation or rolling. This is corroborated by the results on particle concentration, shown in Figure 10 for lower $m^* = 2.5$ kg/kg versus the higher mass loading of the flow, $m^* = 10$ kg/kg. The fluid velocity also is decelerated significantly more close to the bottom wall where more particles reside. In Figures 4 and 6, the results for the average velocity profile and the turbulent energy obtained with the help of typical $k - \varepsilon$ model[35] are also presented by bold

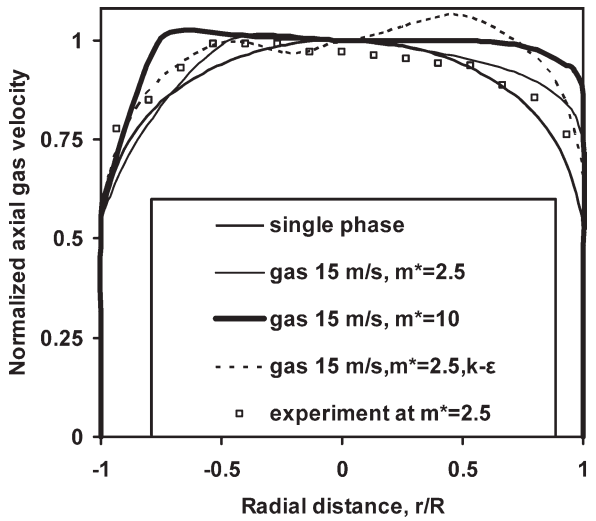

Figure 4. Normalized axial velocity profiles of the gaseous and particulate phases for average velocities of 15 m/s.

The experimental data are from Tsuji and Morikawa.[4]

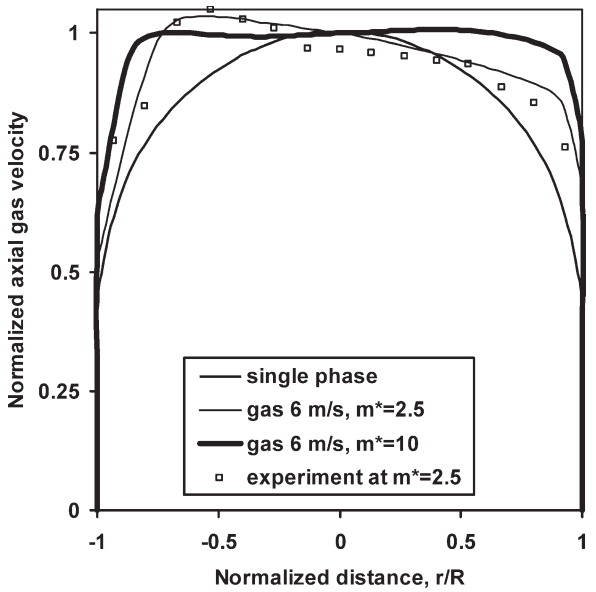

Figure 5. Normalized axial velocity profiles of the gaseous and particulate phases for average velocities of 6 m/s.

The experimental data are from Tsuji and Morikawa.[4]

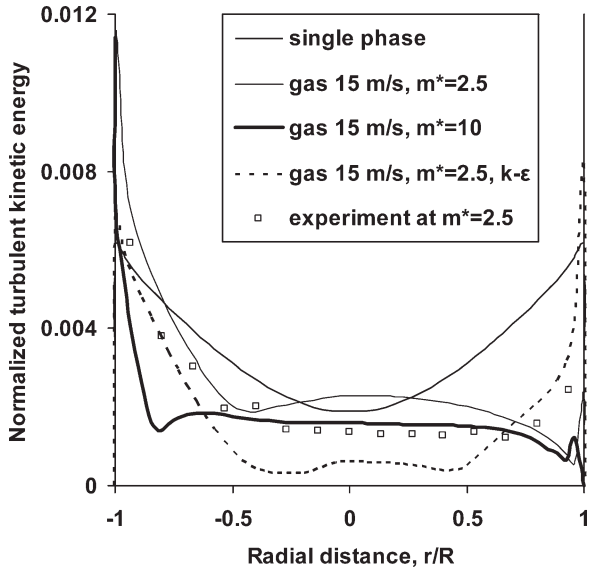

Figure 6. Normalized turbulent kinetic energy profiles for 15 m/s average gas velocities.

The experimental data are from Tsuji and Morikawa.[4]

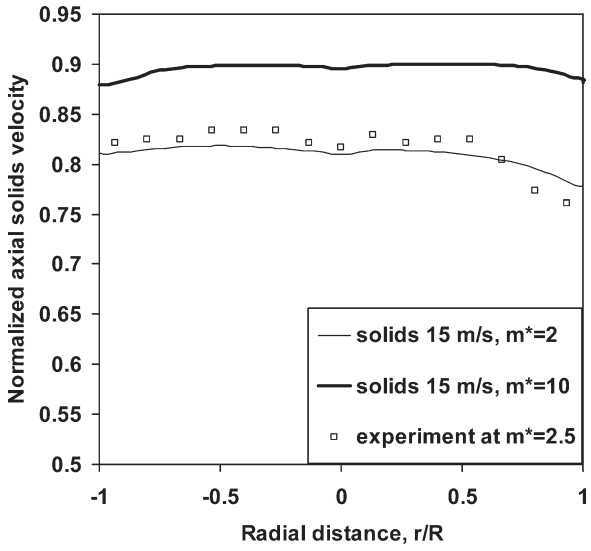

Figure 8. Normalized axial velocity of dispersed phase for 15 m/s average transport velocity.

The experimental data are from Tsuji and Morikawa.[4]

dash lines. It is apparent that the *k–L* model shows better agreement with the experimental data.

The turbulent energy profile shows a similar asymmetry as shown in Figures 6 and 7, which depict the normalized turbulent kinetic energy (turbulence intensity) of the gaseous phase for the two mean flow velocities of gas phase, $\overline{u} = 15$ and 6 m/s. It is observed that there is higher turbulence intensity at the top of the channel than at the bottom, where the higher concentration of the particles occurs. This is due to the lower velocities at the bottom of the channel and the higher attenuation due to the presence of the small particles. As expected in channel flows, the turbulence intensity is significantly higher at the walls and becomes almost uniform in the middle of the channel. Another observation in Figure 6 is that the smaller particles mainly attenuate the turbulence, and thus, the turbulence profile at $m^* = 10$ is lower than at $m^* = 2.5$.

Figure 8 depicts the axial velocity component of the dispersed solids phase in the flow cross section for the case of average gas transport velocity of 15 m/s for two loadings. It may be seen that the velocity profiles of the dispersed phase are almost uniform with slight decreases close to the two walls, where collisions slow down the solids. Again the computations show good agreement with the data by Tsuji and Morikawa.[4]

Figure 9 depicts the radial and azimuthal velocity profiles of the particulate phase for average gas velocity of 15 m/s again for two loadings $m^* = 2.5$ and 10 kg/kg. It is observed that, throughout the channel there is a small but finite azimuthal velocity. The magnitude of the radial velocity is also

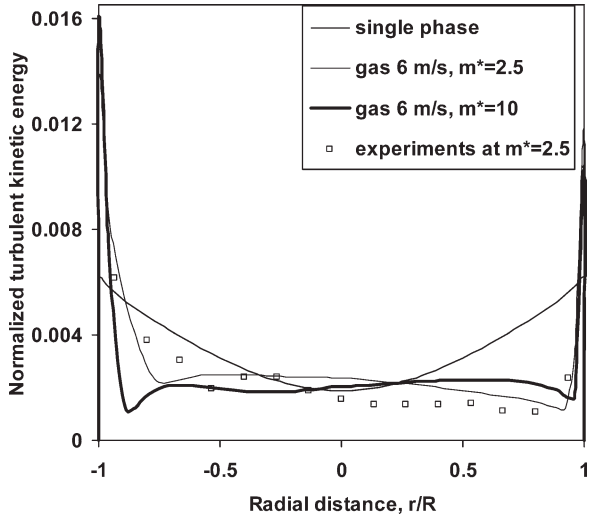

Figure 7. Normalized turbulent kinetic energy profiles for 6 m/s average gas velocities.

The experimental data are from Tsuji and Morikawa.[4]

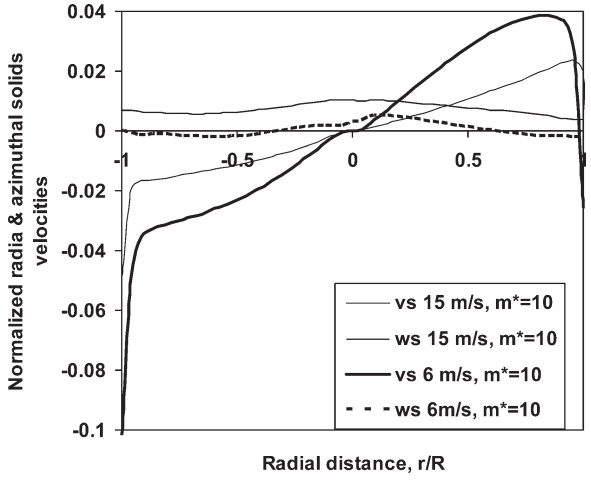

Figure 9. Normalized *r* (radial)- and *z* (azimuthal)-velocity profiles of solids in a horizontal pipe flow for $\overline{u}$ = 15 and 6 m/s and m^* = 10.

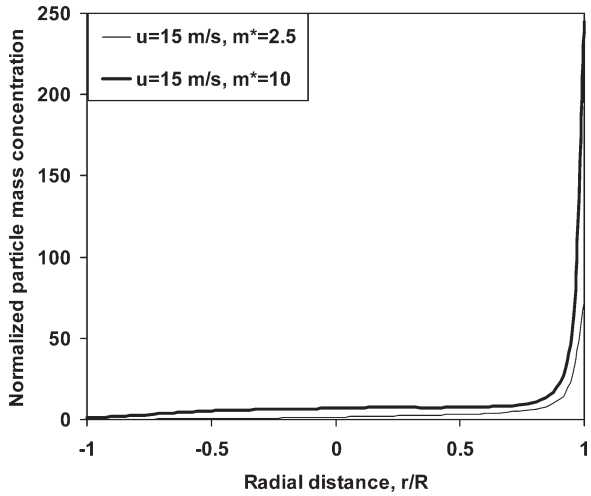

Figure 10. Normalized particle mass concentration profiles for $m^* = 2.5$ and 10 and for $\bar{u} = 15$ m/s.

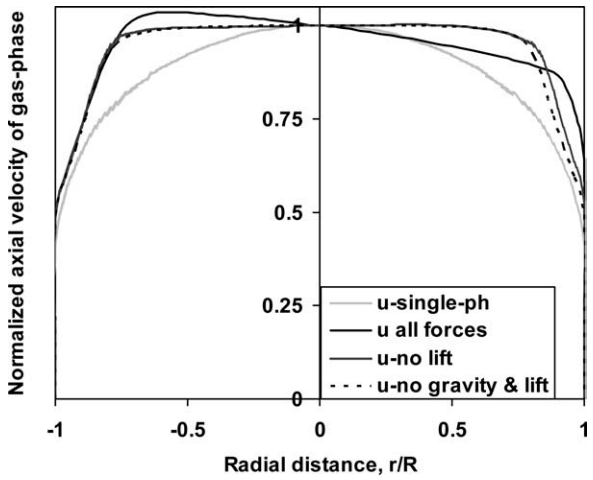

Figure 12. Normalized axial velocity profiles of the gaseous phase for an average velocity of 6 m/s and $m^* = 2.5$ with different force effects.

very low and exhibits the typical profile of radial velocity in channel flow.

Figure 9 shows the normalized radial and azimuthal profiles of the solids velocity. Because the pipe wall is impenetrable, the radial velocity of the dispersed phase should be zero at the top and bottom of the channel if the collisions of the particles were elastic. In this case, we have inelastic collisions with $k_p = 0.95$. This is the cause of the observed jump in the radial velocity component of the dispersed phase close to the two walls. This is also predicted by the relevant boundary condition, Eq. 16. Of course, the magnitude of both normalized radial and azimuthal velocities are much smaller than that of the longitudinal velocity of the dispersed phase. Hence, any contribution of the radial and azimuthal velocities to the transport of solids would be just a perturbation on the average flow.

Figure 10 shows the distribution of particle mass concentration across the cylindrical channel for two cases with $\bar{u} = 15$ m/s and two mass loadings, $m^* = 2.5$ and 10. It is observed that gravity causes the accumulation of particles at the bottom of the pipe.

Figure 11 depicts the distribution of the normalized angular velocity of the solids phase in all three directions. It is observed that the azimuthal average velocity component is an order of magnitude higher than the other components. This occurs because this component of the angular velocity is generated by the axial velocity of the dispersed phase, which is also much higher than two other linear velocity components. It is also observed that this component increases significantly close to the bottom boundary where a great deal of collisions and saltation occur as corroborated by Matsumoto and Saito.[41] There is a slight increase at the top boundary because of the collisions there. This is significantly less pronounced because of the very low concentration of solids at the upper boundary. The figure also shows the azimuthal average velocity component for $m^* = 10$. It is

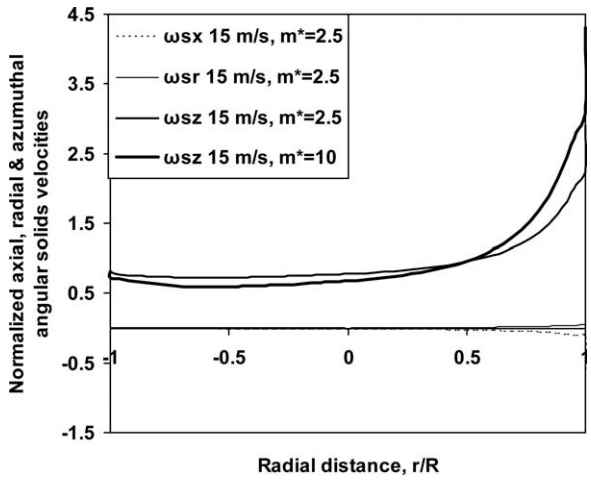

Figure 11. Normalized components of the angular particle velocity.

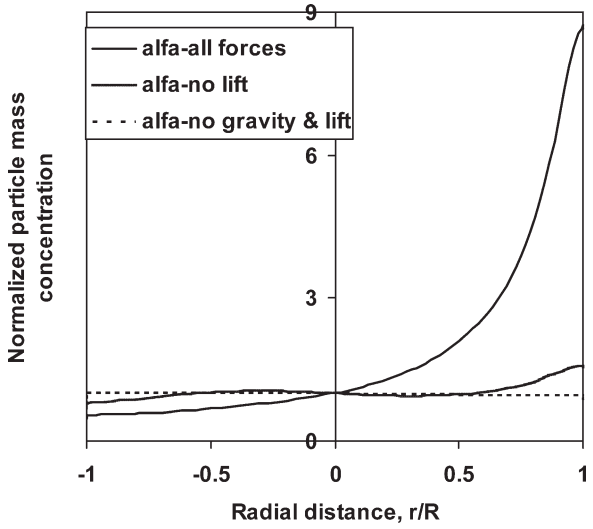

Figure 13. Normalized particle mass concentration profiles for average velocity of 6 m/s and $m^* = 2.5$ with different force effects.

observed that the increase of the loading does not significantly affect this curve.

Figure 12 shows the profiles of the axial velocity and Figure 13 shows the particle mass concentration across the whole length of the flow, that is, from the top wall to the bottom wall for the following three different conditions:

1. When all forces are included in the modeling,
2. when there is no lift force effect in the modeling of the flow, and
3. when there are not lift and gravitation forces.

As one may notice the effect of the lift forces on the shape of the flow profiles in these plots. The impact of the lift forces together with the gravitation force results in an asymmetric distribution of the velocities, the turbulent kinetic energy, and the mass concentration. The absent of gravity forces results, as expected, in symmetrical distributions of particle mass concentration from top to bottom walls.

Conclusions

The full three-dimensional RANS numerical method was developed with the appropriate system of closure equations for the transport of gas–solids mixtures. The model includes the three-dimensional linear momentum interactions as well as angular momentum interactions. Some of the three-dimensional closure equations have been developed from analytical considerations and are used in this study for the first time. The numerical simulation includes the effects lift forces in three dimensions by incorporating the effects of the angular velocity of the particles on the general particle motion. Interparticle collisions particle–wall collisions and similar interactions close to the boundaries are also included in the computations.

The results of the model and the closure equations are reasonable and show very good agreement with available experimental data. It is apparent in all the results that the gas flow becomes asymmetric because of the sedimentation of the particle phase. Also, that the presence of the solid particles has a significant effect on all the flow profiles including the turbulence intensity distribution. One of the advantages of the three-dimensional model, as compared to similar two-dimensional models is that it shows clearly the interactions of the azimuthal and radial components both the linear and the angular velocities.

The three-dimensional two-phase flow modeling is of high relevance for several natural phenomena and engineering processes, where the effects of gravity result to the flow asymmetry. This flow asymmetry cannot be accounted for in two-dimensional models and may be connected to the Boycott effect, density wave propagation, and other physical effects related to the different densities of the two phases.

Acknowledgments

The work in Estonia was done within the framework of "target financing" from Project SF0140070s08 (Estonia) and partially supported by ETF grant Project ETF7620. The work of the second author (E.E.M.) was partly supported by grants from the DOE, DE-NT0008064. Mr. Steven Seachman, Program Manager and by NSF, HRD-0932339, Drs. Demetrios Kazakos and Richard Smith, Program Managers. The authors thank for the technical support of cluster computers at the Universities of Texas at San Antonio and at Austin.

Literature Cited

1. Pfeffer R, Rosetti S, Licklein S. Analysis and correlation of heat transfer coefficient and heat transfer data for dilute gas-solid suspensions. NASA Report Technical Note D-3603, 1966.
2. Michaelides EE. A model for the flow of solid particles in gases. *Int J Multiphase Flow*. 1984;10:61–75.
3. Michaelides EE. *Particles, Bubbles and Drops—Their Motion, Heat and Mass Transfer*. New Jersey: World Scientific Publishing Co. Pte. Ltd., 2006.
4. Tsuji Y, Morikawa Y. LDV measurements of an air-solid two-phase flow in a horizontal pipe. *J Fluid Mech*. 1982;120:385–409.
5. Davies JT. Calculation of critical velocities to maintain solids in suspension in horizontal pipes. *Chem Eng Sci*. 1987;42:1667–1670.
6. Cabrejos FJ, Klinzing GE. Pickup and saltation mechanisms of solid particles in horizontal pneumatic transport. *Powder Technol*. 1994; 79:173–186.
7. Sommerfeld M. Analysis of collision effects for turbulent gas-particle flow in a horizontal channel. I. Particle transport. *Int J Multiphase Flow*. 2003;29:675–699.
8. Sommerfeld M. Validation of a stochastic Lagrangian modelling approach for inter-particle collisions in homogeneous isotropic turbulence. *Int J Multiphase Flow*. 2001;27:1829–1858.
9. Oesterle B, Petitjean A. Simulation of particle to particle interactions in gas-solid flows. *Int J Multiphase Flow*. 1993;19:199–211.
10. Tanaka T, Tsuji Y. Numerical simulation of gas-solid two-phase flow in vertical pipe: on the effect of interparticle collision. In: *4th International Symposium Gas-Solid Flows*, Portland, USA, 1991.
11. Louge MY, Mastorakos E, Jenkins JT. The role of particle collisions in pneumatic transport. *J Fluid Mech*. 1991;231:345–359.
12. Cao J, Ahmadi G. Gas-particle two-phase turbulent flow in vertical duct. *Int J Multiphase Flow*. 1995;21:1203–1228.
13. Gidaspov D. *Multiphase Flow and Fluidization: Continuum and Kinetic Theory Descriptions*. Boston: Academic Press, 1994.
14. Gore RA, Crowe CT. Effect of particle size on modulating turbulent intensity. *Int J Multiphase Flow*. 1989;15:279–285.
15. Yuan Z, Michaelides EE. Turbulence modulation in particulate flows—a theoretical approach. *Int J Multiphase Flow*. 1992;18:779–791.
16. Yarin LP, Hetsroni G. Turbulence intensity in dilute two-phase flows. Parts I, II and III. *Int J Multiphase Flow*. 1994;20:1–44.
17. Crowe CT. On models for turbulence modulation in fluid-particle flows. *Int J Multiphase Flow*. 2000;26:719–727.
18. Guet S, Ooms G, Oliemans RVA. Simplified two-fluid model for gas-lift efficiency predictions. *AIChE J*. 2005;51:1885–1896.
19. Göz MF, Sommerfeld M, Laín S. Instabilities in Lagrangian tracking of bubbles and particles in two-phase flow. *AIChE J*. 2006;52:469–477.
20. Derksen JJ, van den Akker HEA, Sundaresan S. Two-way coupled large-eddy simulations of the gas-solid flow in cyclone separators. *AIChE J*. 2008;54:872–885.
21. Fairweather M, Yao J. Mechanisms of particle dispersion in a turbulent, square duct flow. *AIChE J*. 2009;55:1667–1679.
22. Boycott AE. Sedimentation of blood corpuscles. *Nature*. 1920;104: 532–538.
23. Xu Z-J, Michaelides EE. A numerical simulation of the Boycott effect. *Chem Eng Commun*. 2005;192:532–549.
24. Raafat T, Hulin JP, Hermann HJ. Density waves in dry granular media falling through a vertical pipe. *Phys Rev E*. 1996;53–55:4345–4350.
25. Strauss M, McNamara S, Herrmann HJ. Plug conveying in a horizontal tube. *Granular Matter*. 2007;9:35–48.
26. Kartushinsky A, Michaelides EE. Particle-laden gas flow in horizontal channels with collision effects. *Powder Technol*. 2006;168:89–103.
27. Kartushinsky A, Michaelides EE. Gas-solid particle flow in horizontal channels: decomposition of the particle-phase and interparticle collision effects. *J Fluids Eng*. 2007;129:702–712.
28. Zhu K, Wong CK, Rao SM, Wang CH. Pneumatic conveying of granular solids in horizontal and inclined pipes. *AIChE J*. 2004;50: 1729–1745.

29. Schiller L, Nauman AA. Über die grundlegenden Berechnungen bei der Schwerkraftaufbereitung. *Z Ver Dtsch Ing*. 1933;77:318–320.
30. Tran-Cong S, Gay M, Michaelides EE. Drag coefficients of irregularly shaped particles. *Powder Technol*. 2004;139;21–32.
31. Crowe CT, Sommerfeld M, Tsuji Y. *Multiphase Flows With Droplets and Particles*. Boca Raton, Florida: CRC Press LLC, 1998.
32. Mei R. An approximate expression for the shear lift force on a spherical particle at finite Reynolds number. *Int J Multiphase Flow*. 1992;18:145–147.
33. Kartushinsky A, Michaelides EE. An analytical approach for the closure equations of gas-solid flows with inter-particle collisions. *Int J Multiphase Flow*. 2004;30:159–180.
34. Pourahmadi F, Humphrey JAC. Modeling solid-fluid turbulent flows with application to predicting erosive wear. *Phys Chem Hydrodyn*. 1983;4:191–219.
35. Shraiber AA, Yatsenko VP, Gavin LB, Naumov VA. *Turbulent Flows in Gas Suspensions*. New York: Hemisphere Publishing Corp., 1990.
36. Zaichik LI, Alipchenkov VM. Statistical models for predicting particle dispersion and preferential concentration in turbulent flows. *Int J Heat Fluid Flow*. 2005;26:416–430.
37. Happel J, Brenner H. *Low Reynolds Number Hydrodynamics*. Leiden: Noordhoff International Publishing, 1973.
38. Perić M, Scheuerer G. CAST—a finite volume method for predicting two-dimensional flow and heat transfer phenomena. GRS—Technische Notiz SRR, 1989.
39. Ferziger JH, Perić M. *Computational Methods for Fluid Dynamics*. New York: Springer-Verlag, 1995.
40. Ding J, Lyczkowski RW, Sha WT, Altobelli SA, Fukushima E. Numerical analysis of liquid-solids suspension velocities and concentrations obtained by NMR imaging. *Powder Technol*. 1993;77:301–312.
41. Matsumoto S, Saito SJ. Monte Carlo simulation of horizontal pneumatic conveying based on the rough wall model. *J Chem Eng Jpn*. 1970;3:223–230.

Manuscript received Oct. 14, 2009, revision received Oct. 8, 2010, and final revision received Dec. 16, 2010.